Contrib Mineral Petrol (2015) 169:1088
DOI 10.1007/s00410-014-1088-1

ORIGINAL PAPER

The age of Au–Cu–Pb-bearing veins in the poly-orogenic Ubendian Belt (Tanzania): U–Th–total Pb dating of hydrothermally altered monazite

Emmanuel Owden Kazimoto · Volker Schenk · Peter Appel

Received: 2 April 2014 / Accepted: 12 November 2014
© Springer-Verlag Berlin Heidelberg 2014

Abstract The age of gold–copper–lead mineralization in the Katuma Block of the Ubendian Belt remains controversial because of the lack of radiometric ages that correlate with the age of tectonothermal events of this poly-orogenic belt. Previous studies reported whole rock and mineral Pb–Pb ages ranging between 1,660 and 720 Ma. In this study, we report U–Th–total Pb ages of monazite from hydrothermally altered metapelites that host the Au–Cu–Pb-bearing veins. Three types of chemically and texturally distinct types of monazite grains or zones of grains were identified: monazite cores, which yielded a metamorphic age of 1,938 ± 11 Ma ($n = 40$), corresponding to known ages of a regional metamorphic event, deformation and granitic plutonism in the belt; metamorphic overgrowths that date a subsequent metamorphic event at 1,827 ± 10 Ma ($n = 44$) that postdates known eclogite metamorphism (at ca. 1,880 Ma) in the belt; hydrothermally altered poikilitic monazite, formed by dissolution–precipitation processes, representing the third type of monazite, constrain the age of a hydrothermal alteration event at 1,171 ± 17 Ma ($n = 19$). This Mesoproterozoic age of the hydrothermal alteration coincides with the first amphibolite grade metamorphism of metasediments in the Wakole Block, which adjoins with a tectonic contact the vein-bearing Katuma Block to the southwest. The obtained distinct monazite ages not only constrain the ages of metamorphic events in the Ubendian Belt, but also provide a link between the metamorphism of the Wakole metasediments and the generation of the hydrothermal fluids responsible for the formation of the gold–copper–lead veins in the Katuma Block.

Keywords Monazite dating · Kibaran orogeny · Crustal thickening · Orogenic gold mineralization · Hydrothermally altered monazite

Communicated by O. Müntener.

Electronic supplementary material The online version of this article (doi:10.1007/s00410-014-1088-1) contains supplementary material, which is available to authorized users.

E. O. Kazimoto (✉) · V. Schenk · P. Appel
Institut für Geowissenschaften, Christian-Albrechts-Universität Kiel, Ludewig-Meyn-Str. 10, 24118 Kiel, Germany
e-mail: ekazimoto@gmail.com; ekazimoto@udsm.ac.tz

E. O. Kazimoto
Department of Geology, University of Dar es Salaam, P. O. Box 35052, Dar es Salaam, Tanzania

Introduction

Despite many attempts and its importance in exploration, dating of hydrothermal gold mineralization in orogenic belts is still a challenge due to the scarcity of minerals formed during mineralization that are suitable for dating. Additional difficulties for dating arise from the fact that mineralized zones are formed by multiple episodes of mineralization and postdepositional hydrothermal alterations; this results in a wide range of scattering dates. Attempts to date, mineralization events using hydrothermally altered minerals of the adjoining country rocks may also result in ambiguous, mixed ages due to incomplete resetting of the applied isotopic systems. The geochronological methods used to date mineralization include $^{40}Ar/^{39}Ar$ dating of hydrothermal minerals (e.g., adularia, biotite, K-feldspar and white mica) and mica inclusion in hydrothermal sulfides (Phillips and Miller 2006), Re–Os dating of sulfide minerals (e.g., molybdenite, arsenopyrite, pyrite and chalcopyrite) associated with gold mineralization (Arne et al. 2001; Lawley et al. 2013c; Selby et al. 2002; Stein et al.

Published online: 26 November 2014

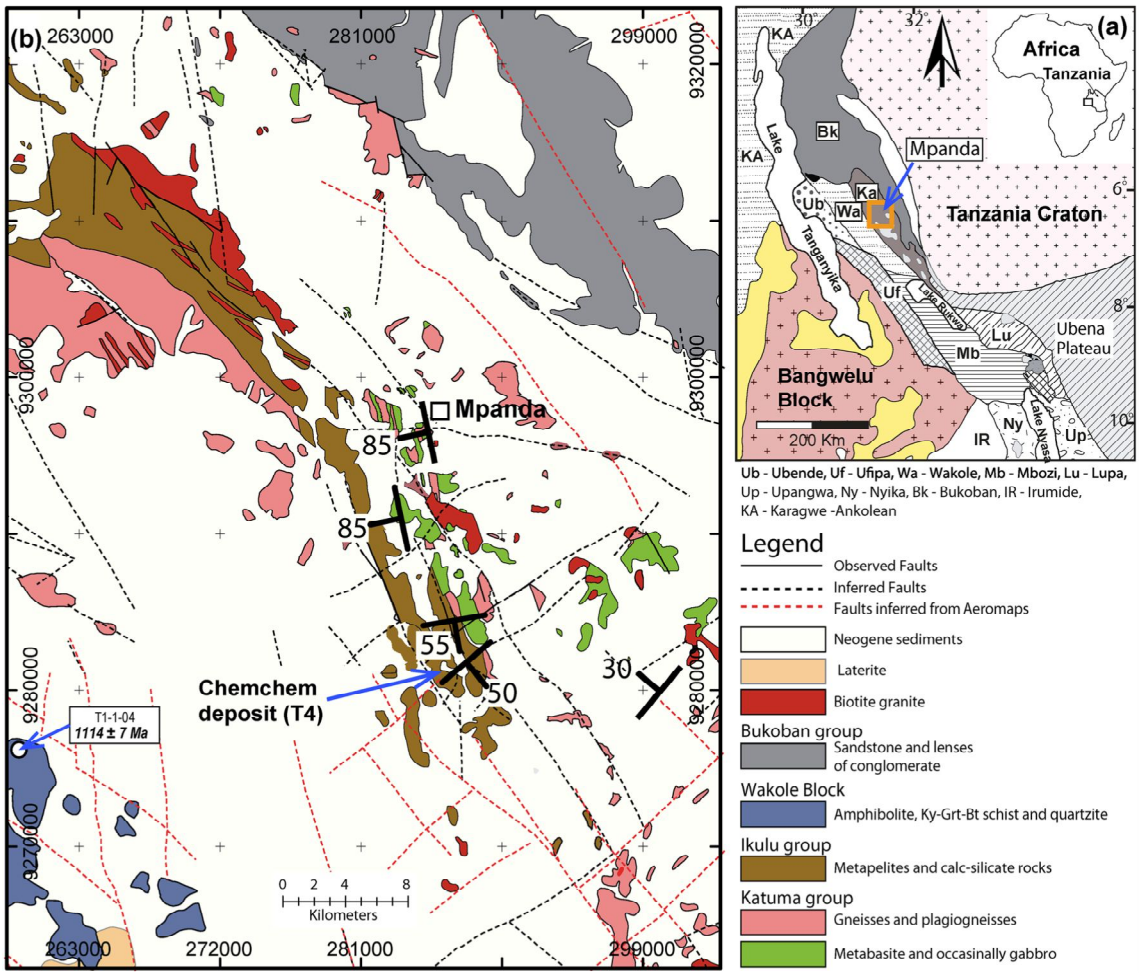


Fig. 1 **a** Regional geological map showing the geological setting of the Paleoproterozoic Ubendian Belt, its blocks and bordering belts (modified after Pohl 1994 and Daly 1988). **b** Geological map of Katuma Block modified after Biyashev et al. (1977), Semyanov et al. (1977) and Smirnov et al. (1970). The age of the Wakole metasedimentary rocks is from Boniface et al. (2014)

2001), Pb–Pb dating of hydrothermal sulfides (Frei and Pettke 1996) and U–Pb and Pb–Pb dating of hydrothermally formed zircon and monazite (Davis et al. 1994; Hu et al. 2004; Rasmussen et al. 2006; Vielreicher et al. 2003; Kerrich et al. 1994).

Knowledge of the age of mineralization or of a hydrothermal event is a prerequisite to understanding its relation with the tectonic, magmatic or metamorphic events during an orogenic cycle. The formation of hydrothermal deposits is often coeval with the accretion of tectonic terranes and therefore, on a global scale, is often related to the amalgamation of supercontinents (Barley and Groves 1992; Kerrich et al. 1994). In addition to this coeval mineralization, Kerrich and Cassidy (1994) noted that some vein deposits are up to 250 Ma younger than the primary orogenic events and seem not to be related to the orogenic evolution. The different age relationships between the mineralization and the orogenic evolution have been referred to as "early gold" and "late gold" models.

The Paleoproterozoic Ubendian Belt (2.1–1.8 Ga), which was formerly interpreted as an entirely Paleoproterozoic Belt (Daly 1988; Lenoir et al. 1994), has been recently recognized to be affected by three orogenic cycles: the Paleoproterozoic Ubendian, the Mesoproterozoic Kibaran and the Neoproterozoic Pan-African events (Boniface et al. 2012, 2014; Boniface and Schenk 2012). These events did not affect the entire Ubendian Belt with the same intensity but were, in part, localized. For example, the Mesoproterozoic event affected only the northern parts of the belt north of a Neoproterozoic suture (Boniface et al. 2014; Boniface and Schenk 2012). The Paleoproterozoic Ubendian Belt contains also two orogenic gold deposits (Goldfarb et al. 2001): one in the Lupa Block (Lawley et al. 2013a, c, d) and a second in the Mpanda mineral field in the Katuma Block (Fig. 1a, b). Attempts to date, the Mpanda gold mineralization with the Pb–Pb method used galena, chalcopyrite, pyrite and Cu–Au-oxidized

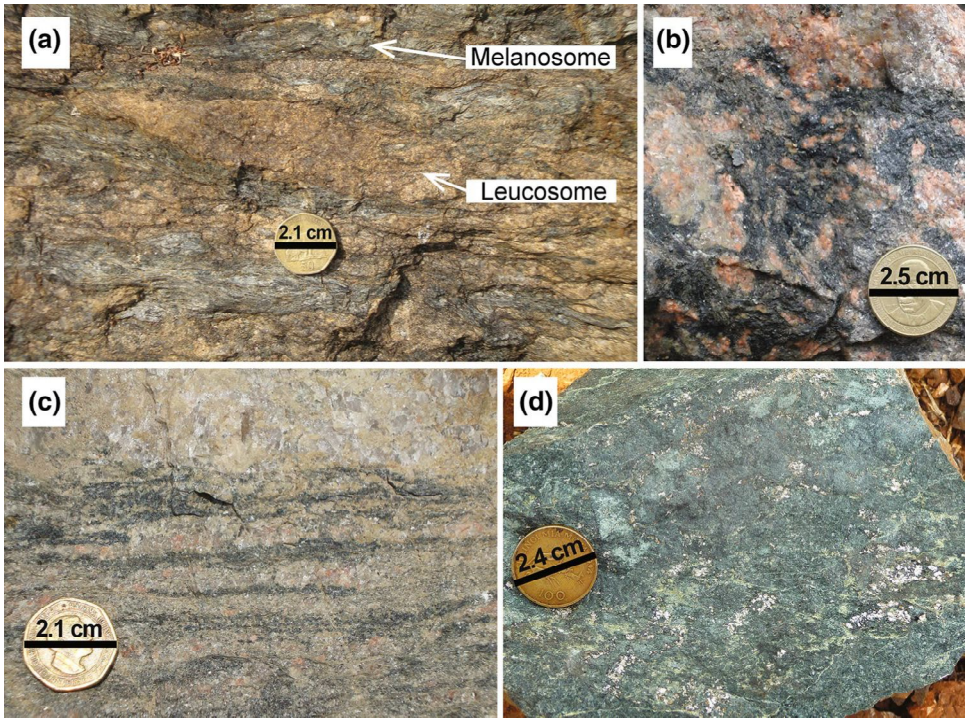


Fig. 2 **a** Ikulu metapelite at Chemchem mine showing mafic bands (Bt-Sil) and felsic bands (Qz-Fsp). **b** K-feldspar alteration of the Ikulu metapelite adjacent to the Au–Cu-bearing veins at Chemchem mine. **c** Epidote–K-feldspar–sericite alteration of Ikulu metapelite adjacent to the Au–Cu–Pb-bearing veins at Chemchem mine. **d** Chlorite–epidote–pyrite alteration of amphibolite adjacent to a gold-bearing vein

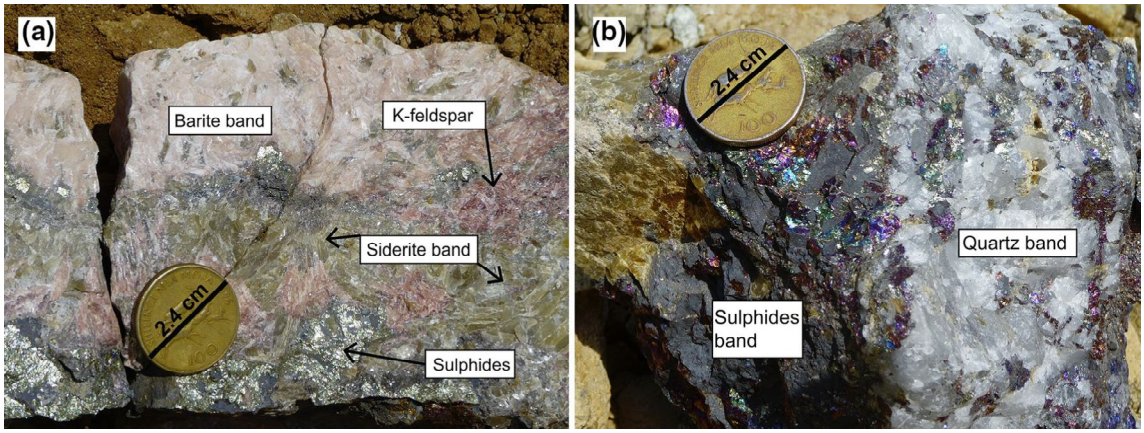


Fig. 3 **a** A photo of ores from Singililwa Au–Cu mine that consist of barite, K-feldspar, siderite and pyrite. **b** Another type of ore primarily composed of quartz and sulfides (pyrite and chalcopyrite)

ores, which resulted in a wide range of ages between 1660 and 720 Ma (Cahen et al. 1966; Nanyaro 1989; Stendal et al. 2004). This range indicates that the mineralization in Mpanda cannot be regarded as an "early gold" mineralization with respect to the Paleoproterozoic (2.1–1.8 Ga) orogenic evolution of the belt. Stendal et al. (2004) first classified this mineralization event as late gold of post-Paleoproterozoic age, using the Pb–Pb isotope compositions of whole rocks and sulfides. According to these authors, the mineralization was contemporaneous with the emplacement of a alkali granite and the Sangu–Ikola carbonatite (ca. 720 Ma) within the Ubendian Belt, in which the Paleoproterozoic orogenic evolution ended with collision and eclogite formation at about 1.84 Ga. In view of the new findings that suggest three orogenic cycles to have affected the Ubendian Belt, the interpretation of the origin of the Mpanda gold mineralization, its age and its correlation with the complex orogenic evolution of the belt warrants reevaluation.

In the present study, we dated a mineral of which we assume that it formed or recrystallized during the hydrothermal mineralization event due to fluid

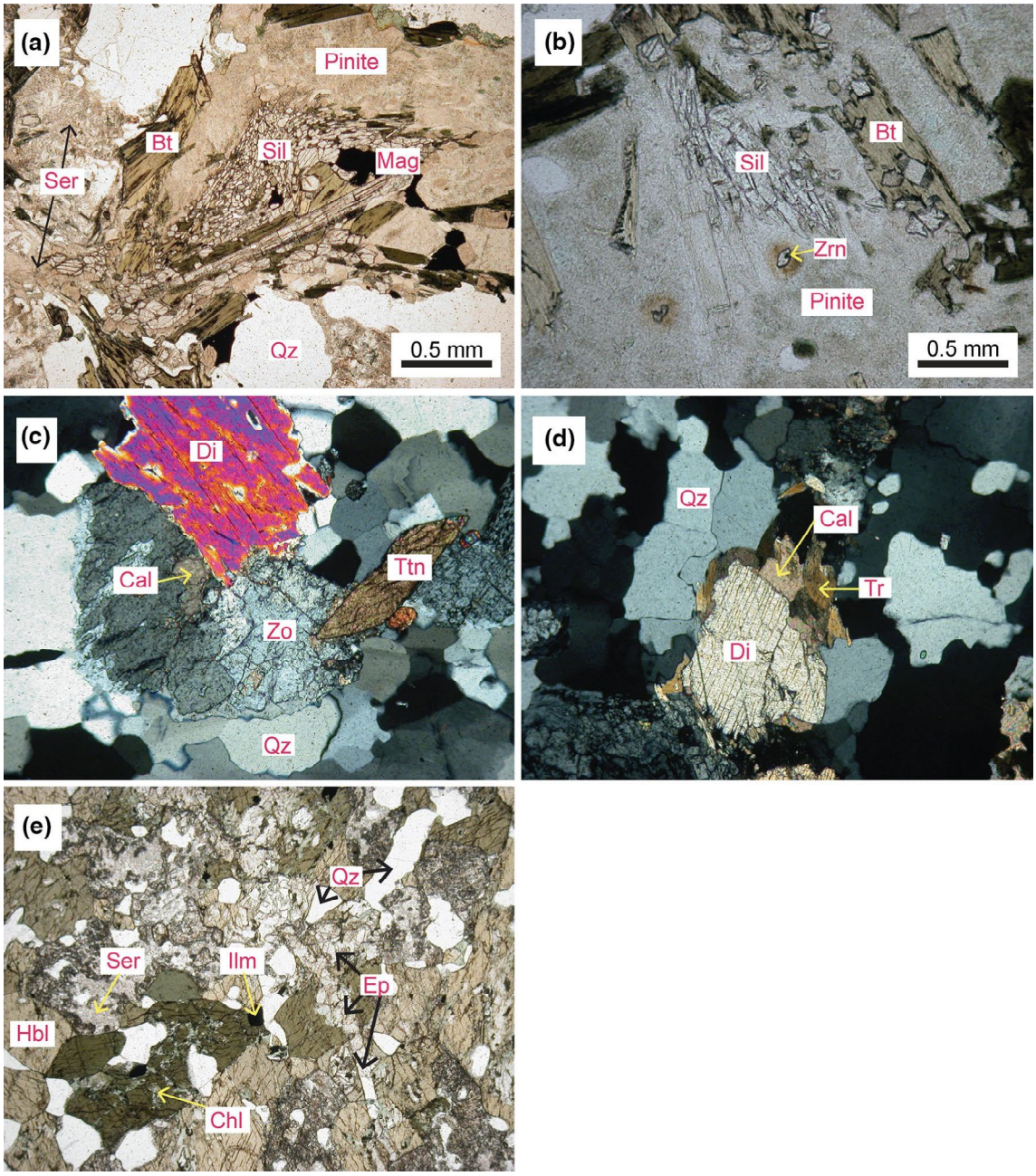


Fig. 4 Photomicrograph of various rock types from the Chemchem mine in plane-polarized light (**a**, **b**). Photomicrograph of the metapelite showing sillimanite cluster and biotite surrounded by pinite pseudomorph after cordierite and **b** zircon grains surrounded by pleochroic halos within the pinite. **c**, **d** Photomicrograph of the calc-silicate rock showing diopside (*Di*) and quartz (*Qz*) partly replaced by tremolite (*Tr*), calcite (*Cal*), zoisite (*Zo*) and titanite (*Ttn*). **e** Photomicrograph of the metabasite depicting an assemblage of hornblende (*Hbl*), plagioclase (*Pl*), ilmenite (*Ilm*) and quartz (*Qz*) replaced by chlorite (*Chl*), sericite (*ser*) and epidote (*Ep*)

infiltration into the metapelitic country rocks of the gold-bearing veins. We employed electron microprobe U–Th–total Pb dating of hydrothermally altered monazite present in hydrothermally altered metapelites. The age of the hydrothermally altered monazite obtained in this way is in accordance with reported ages of the first metamorphism of the precursor pelitic sediments of the adjoining Wakole Block. This result suggests that the gold mineralization in the Katuma Block occurred during the Mesoproterozoic Kibaran orogeny and lends support to an "early gold" orogenic deposit model. Moreover, our study demonstrates the successful use of hydrothermally altered monazite in dating a metallic hydrothermal mineralization.

Geological setting

The Ubendian Belt

The Paleoproterozoic Ubendian Belt is a NW–SE-trending metamorphic belt located along the southwest margin of the Archean Tanzania Craton, separating the craton from the Bangweulu Block and the Mesoproterozoic Irumide Belt to the southwest. The northern part of the belt is unconformably overlain by metamorphosed to unmetamorphosed sedimentary rocks of the Mesoproterozoic Karagwe-Ankolean Belt and the Meso- to Neoproterozoic Bukoban Supergroup (Fig. 1a). The belt has been subdivided into eight lithologically distinct blocks, namely the Ubende, Wakole, Katuma, Ufipa, Mbozi, Lupa, Upangwa and Nyika Blocks (Fig. 1a), which are separated by NW–SE-trending zones of mylonite, ultra-mylonite and gouge that exhibit a dextral sense of shear (Daly 1988).

The Ubendian Belt is associated with a complex structural and metamorphic history that spans from the Paleoproterozoic to the Neogene; therefore, the belt has been considered to be a crustal zone of a persistent structural weakness (Boven et al. 1999; Kilembe and Rosendahl 1992; Lenoir et al. 1994; Theunissen et al. 1996; Delvaux 2001). The early Paleoproterozoic tectono-thermal events have been assigned to two separate stages. The first stage (~2.1–2.0 Ga) is characterized by felsic and mafic magmatism and granulite facies metamorphism that was locally, along shear zones, followed by a greenschist facies overprint and an E–W-striking tectonic rock fabric (Lawley et al. 2013b, c; Lenoir et al. 1994; Ring et al. 1997). The second stage (1.9–1.83 Ma) is associated with the formation of eclogites that formed from subducted oceanic crust (Boniface et al. 2012), besides amphibolites and granulites, NW–SE block-bounding shear zones and an orogenic gold deposit in the Lupa Block (Boniface et al. 2012; Lenoir et al. 1994; Lawley et al. 2013b, c). The Mesoproterozoic tectono-thermal events were recorded by zircon and monazite in the rocks of the blocks located in the northern part of the Ubendian Belt (Katuma, Ubende and Wakole Blocks) (Boniface et al. 2014, 2012). Only in the Wakole Block, both zircon and monazite indicate that the metasediments were first metamorphosed during Mesoproterozoic events (1,170 and 1,010 Ma) due to crustal thickening (Boniface et al. 2014). A second group of eclogites in the Ubendian Belt that display volcanic-arc chemistry and occur in the Ufipa Block mark the location of a Neoproterozoic suture zone (ca. 590–520 Ma) that formed due to the amalgamation of the Gondwana supercontinent, when the Ubendian Belt was the site of volcanic-arc accretion and suturing between the Bangweulu Block and the Tanzania Craton (Boniface and Schenk 2012). The northwestern faults of the East African Rift along the Ubendian Belt suggest a young rift-related reactivation of the older Precambrian zones of weakness (Kilembe and Rosendahl 1992; Theunissen et al. 1996).

Katuma Block

The Katuma Block is located on the northern margin of the Ubendian Belt and is bounded by the Archean Tanzania Craton in the northeast and the Wakole Block in the southwest (Fig. 1a). The rocks in this block are divided into two groups (Fig. 1b). The Katuma Group is mainly composed of schistose to migmatitic orthogneisses and metabasites that are locally associated with non-metamorphic gabbronorites. The Ikulu Group, for which a thickness of ca. 1.4 km has been estimated, unconformably overlies the Katuma Group and is composed mainly of metasedimentary rocks (Semyanov et al. 1977). Gold-bearing veins cut the rocks of the Katuma and the Ikulu Group and are associated with hydrothermal alteration of the adjoining rocks. The country rocks of the veins at Chemchem include aluminous metapelites, calc-silicates of amphibolite-to granulite facies grade. These rocks are assumed to have experienced only high-grade Paleoproterozoic metamorphic events but no low-grade regional metamorphic overprint at the time of the vein formation. The hydrothermal alteration of metapelites and metabasites includes the formation of chlorite, sericite, epidote, quartz and calcite (Fig. 2b–d). Plagioclase and K-feldspar are altered to white micas. Light gray K-feldspar is becoming red in color by the alteration (Fig. 2b). The veins are composed of siderite, barite, quartz, K-feldspar and sulfides (primarily pyrite and chalcopyrite and/or galena), and the gold is primarily hosted in pyrite and chalcopyrite (Fig. 3a, b).

The veins display two major orientational trends: parallel to the strike of the rocks (NW–SE) and nearly perpendicular to the strike (NE–SW and E–W) (Fig. 1b). The NW–SE shear and fracture zones are thought to have formed during the latest Paleoproterozoic Ubendian tectonic event (ca. 1.80 Ga; Stendal et al. 2004; Lenoir et al. 1994), whereas the E–W-trending veins are associated with the early Paleoproterozoic event (ca. 2.1–2.0 Ga) and the Neoproterozoic reactivation (Stendal et al. 2004). An interpretation of aeromagnetic data indicates primarily a structural control of the mineralized veins along the NW–SE border between the Katuma and Ikulu Group (Stendal et al. 2004).

Analytical methods

Samples of the Ikulu metapelites were collected adjacent to a Au–Cu–Pb-bearing vein in the Chemchem Cu–Au abandoned mine in Mpanda (Fig. 1b). The mineral analyses and in

Table 1 Representative electron microprobe analyses of different minerals in metapelite, calc-silicate rocks and metabasite

Mineral analysis #	Metapelite								Calc-silicate rock									
	Bt	Bt	Ms	Ms	Chl	Chl	Pl	Pl	Cpx	Cpx	Tr	Tr	Zo	Zo	Pl	Pl	Ms	Ms
	865	867	579	583	960	962	918	920	605	626	20	30	750	751	73	74	766	768
SiO_2	35.64	35.34	45.17	45.42	26.04	28.22	60.13	60.51	55.08	54.95	58.24	58.82	39.77	39.46	66.59	67.00	47.08	47.18
TiO_2	2.72	2.60	0.87	0.72	0.00	0.00	0.00	0.00	0.01	0.07	0.05	0.11	n.d	n.d	0.00	0.00	n.d	n.d
Al_2O_3	18.49	18.47	34.24	34.19	21.32	20.48	25.50	24.96	0.55	0.52	1.56	0.99	34.50	34.68	20.94	20.58	34.45	34.46
Cr_2O_3	0.04	0.06	0.06	0.06	0.01	0.00	n.d	n.d	0.00	0.00	0.00	0.00	n.d	n.d	0.00	0.00	n.d	n.d
Fe_2O_3	n.c	n.c	n.c	n.c	n.c	n.c	0.07	0.13	n.c	n.c	n.c	n.c	0.06	0.10	n.c	n.c	n.c	n.c
FeO	16.85	17.46	2.28	2.41	22.99	22.65	0.00	0.00	0.18	0.20	0.38	0.46	0.05	0.09	0.00	0.01	0.00	0.10
MnO	0.25	0.15	0.03	0.02	0.28	0.28	n.d	n.d	0.06	0.01	0.01	0.00	n.d	n.d	0.00	0.00	n.d	n.d
MgO	11.80	11.63	0.58	0.56	17.30	16.52	n.d	n.d	18.38	18.31	23.65	24.20	n.d	n.d	0.00	0.00	n.d	n.d
CaO	0.00	0.01	0.00	0.00	0.01	0.04	6.03	5.83	25.60	25.83	13.58	13.74	24.49	24.68	1.44	1.16	0.12	0.08
Na_2O	0.17	0.22	0.52	0.55	0.01	0.56	8.13	8.50	0.14	0.11	0.17	0.10	0.06	0.02	10.84	11.14	0.23	0.22
K_2O	10.34	9.99	11.23	11.05	0.00	0.00	0.12	0.09	0.00	0.00	0.05	0.01	0.01	0.00	0.11	0.10	11.85	11.79
Total	96.29	95.94	94.98	94.98	87.96	88.75	99.99	100.02	99.99	99.99	97.69	98.43	98.89	98.94	99.99	99.99	93.73	93.83
Structural formulae																		
Si	2.67	2.66	6.11	6.13	5.40	5.77	2.68	2.68	1.99	1.98	7.90	7.92	2.98	2.96	2.92	2.94	6.36	6.36
Ti	0.15	0.15	0.09	0.07	0.00	0.00	0.00	0.00	0.00	0.00	0.00	0.01	0.00	0.00	0.00	0.00	5.48	5.48
Al	1.63	1.64	5.46	5.44	5.21	4.93	1.32	1.34	0.02	0.02	0.25	0.16	3.05	3.06	1.08	1.06	0.00	0.00
Cr	0.00	0.00	0.01	0.01	0.00	0.00	n.d	n.d	0.00	0.00	0.00	0.00	n.d	n.d	0.00	0.00	n.d	n.d
Fe^{3+}			n.c	n.c	n.c	n.c	0.00	0.00	n.c	n.c	n.c	n.c	0.00	0.01	n.c	n.c	n.c	n.c
Fe^{2+}	1.06	1.10	0.26	0.27	3.99	3.87	n.c	n.c	0.01	0.01	0.04	0.05	n.c	n.c	0.00	0.00	0.00	0.01
Mn	0.02	0.01	0.00	0.00	0.05	0.05	n.d	n.d	0.00	0.00	0.00	0.00	n.d	n.d	0.00	0.00	n.d	n.d
Mg	1.32	1.31	0.12	0.11	5.35	5.03	n.d	n.d	0.99	0.99	4.78	4.86	n.d	n.d	0.00	0.00	n.d	n.d
Ca	0.00	0.00	0.00	0.00	0.00	0.01	0.29	0.29	0.99	1.00	1.97	1.98	1.97	1.98	0.07	0.05	0.02	0.01
Na	0.02	0.03	0.14	0.14	0.00	0.22	0.72	0.70	0.01	0.01	0.04	0.03	0.01	0.00	0.92	0.95	0.06	0.06
K	0.99	0.96	1.94	1.90	0.00	0.00	0.01	0.01	0.00	0.00	0.01	0.00	0.00	0.00	0.01	0.01	2.04	2.03
Total	7.86	7.86	18.11	18.09	20.00	19.88	5.02	5.01	4.01	4.01	15.00	15.00	8.00	8.01	5.00	5.01	13.96	13.94
Oxygen	11	11	22	22	28	28	8	8	6	6	23	23	8	8	8	8	22	22
XFe	0.44	0.46	0.69	0.71	0.43	0.43												

	Metabasite									
	Hbl	Hbl	Pl	Pl	Ep	Ep	Act	Act	Ms	Ms
	308	310	356	362	364	366	425	426	330	333
SiO_2	44.32	44.25	53.98	54.52	38.28	38.31	44.56	44.25	48.23	47.63
TiO_2	1.06	0.96	0.00	0.00	0.04	0.13	0.78	0.81	0.01	0.00
Al_2O_3	10.60	10.55	29.27	28.59	25.49	26.23	10.43	10.48	32.12	31.40
Cr_2O_3	0.07	0.04	0.00	0.00	0.07	0.05	0.05	0.03	0.00	0.00
Fe_2O_3	n.c	n.c	n.c	n.c	n.c	n.c	n.c	n.c	n.c	n.c
FeO	17.98	18.17	0.16	0.18	9.70	8.63	18.14	17.80	2.73	2.80
MnO	0.39	0.39	0.00	0.00	0.14	0.11	0.41	0.34	0.04	0.05
MgO	10.26	10.26	0.00	0.00	0.02	0.03	9.98	10.14	1.15	1.86
CaO	11.08	10.80	11.64	11.09	23.47	23.78	10.86	11.05	0.09	0.04
Na_2O	1.34	1.33	4.95	5.41	0.00	0.01	1.32	1.49	0.22	0.14
K_2O	0.70	0.72	0.02	0.03	0.01	0.00	0.67	0.68	11.17	11.32
Total	97.80	97.47	100.03	99.88	97.22	97.27	97.20	97.06	95.77	95.24
Structural formulae										
Si	6.65	6.66	2.44	2.47	3.26	3.22	6.72	6.68	6.44	6.42
Ti	0.12	0.11	0.00	0.00	0.00	0.01	0.09	0.09	0.00	0.00
Al	1.87	1.87	1.56	1.52	2.55	2.60	1.85	1.87	5.06	4.99
Cr	0.01	0.00	0.00	0.00	n.c	n.c	0.01	0.00	0.00	0.00
Fe^{3+}	n.c	n.c	n.c	n.c	0.00	0.00	n.c	n.c	n.c	n.c

Table 1 continued

	Metabasite									
	Hbl	Hbl	Pl	Pl	Ep	Ep	Act	Act	Ms	Ms
	308	310	356	362	364	366	425	426	330	333
Fe^{2+}	2.26	2.29	0.01	0.01	n.c	n.c	2.29	2.25	0.30	0.32
Mn	0.05	0.05	0.00	0.00	0.01	0.01	0.05	0.04	0.00	0.01
Mg	2.29	2.30	0.00	0.00	0.00	0.00	2.24	2.28	0.23	0.37
Ca	1.78	1.74	0.56	0.54	2.14	2.14	1.75	1.79	0.01	0.01
Na	0.39	0.39	0.43	0.48	0.00	0.00	0.39	0.44	0.06	0.04
K	0.13	0.14	0.00	0.00	0.00	0.00	0.13	0.13	1.90	1.95
Total	15.55	15.56	5.00	5.01	7.96	7.98	15.52	15.57	14.01	14.08
Oxygen	23	23	8	8	8	8	23	23	22	22

n.c not calculated, *n.d* not determined

situ U–Th–total Pb monazite dating were performed using a JEOL Superprobe JXA-8900R Electron Probe Microanalyzer at the Institute of Geoscience of the University of Kiel. For the biotite, plagioclase, amphiboles, epidote, zoisite, muscovite and chlorite analysis, analyses were performed using an accelerating voltage of 15 kV and a probe current of 15 or 20 nA. Synthetic and natural mineral standards were used and the CITZAF method of Armstrong (1995) was applied for matrix correction. Except for minor differences in the values of accelerating potential and probe current, the in situ U–Th–total Pb monazite dating was performed using procedures similar to those described by Braun and Appel (2006) and Jöns et al. (2006). The U–Th–total Pb contents of the monazite were determined using an accelerating voltage of 20 kV and a probe current of 60 or 80 nA. The microprobe was calibrated for P, REE and Y using the synthetic REE orthophosphate standards of the Smithsonian Institute (Jarosewich and Boatner 1991). The composition of these standards was carefully determined considering their Pb content (see Donovan et al. 2003). For Th, Pb, U, Si, Ca and Al analysis, the microprobe was calibrated using thorianite, crocoite, synthetic U-bearing glasses, wollastonite and corundum, respectively. The JEOL ZAF program was used for matrix correction. Counting times for Pb are between 2 and 4 min on the peak and similar times on the background, depending on the intensities. The Pb–Mb lines, Th–Ma lines and U–Mb lines (considering interference from Y Mg) were used. More details about the analytical protocol and the background approximation for Pb are given at http://www.ifg.uni-kiel.de/1202.html. The quality of the data was controlled by repeated analyses of two Manangotry monazite grains from southeast Madagascar (sampled and kindly provided by Michael Raith, Bonn). The analytical distance on monazite grains was about 10 μm. These reference materials are homogenous in composition (e.g., Electronic Supplementary Table 1; Horstwood et al. 2003; Oelkers and Poitrasson 2002) and were dated by Horstwood et al. (2003) and Paquette and Tiepolo (2007) at 555 ± 1 and 555 ± 2 (upper intercept). The obtained compositions and ages of Manangotry monazite (Electronic Supplementary Table 1) are within errors similar to those reported by Oelkers and Poitrasson (2002), Horstwood et al. (2003) and Paquette and Tiepolo (2007), respectively. Analyses with significant apparent Al contents were rejected to avoid artifacts from secondary fluorescence that may occur if analytical points are too close to grain boundaries. The chemical ages of the monazite together with their uncertainties were then calculated using the "Comb-error" and "AgeFinder" software programs (Appel 2010, 2013).

Petrography and mineral chemistry

In the surroundings of the abandoned Chemchem mine, three major rock types occur. These are metapelites, which host the hydrothermal veins and the dated monazites and show strong alteration besides unaltered calc-silicate rocks and little-altered amphibolites. To characterize the prograde metamorphic state of these rocks in relation to the conditions during the alteration and to characterize the degree of alteration, the petrography of different rock types is described below.

Ikulu metapelite

Ikulu metapelites containing the dated hydrothermally altered monazite are gneissic to migmatitic in texture (Fig. 2a) and contain assemblages of biotite, sillimanite, cordierite, plagioclase, quartz and K-feldspar (Fig. 4a, b). The biotite and sillimanite are primarily present in the melanosomes, and quartz, plagioclase and K-feldspar are primarily present in the leucosomes. Under the microscope, the biotite is green to brownish green and is surrounded by retrograde exsolution of ilmenite along its rims. The sillimanite is present in common clusters, which on the basis

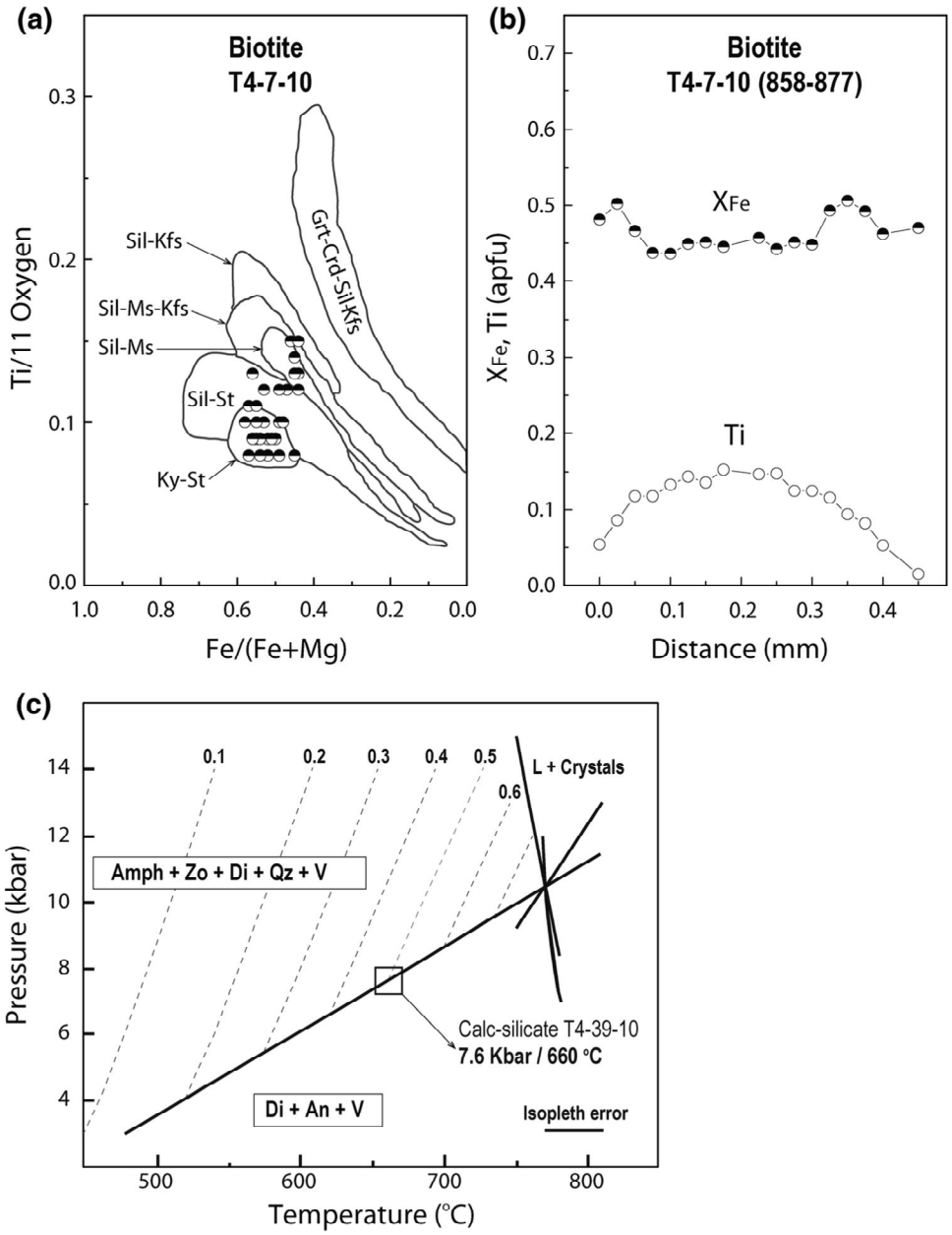


Fig. 5 **a** Plot of Ti (per 11 oxygens) versus Fe/(Fe+Mg) for biotite of the Ikulu metapelite hosting gold-bearing veins. The fields are compositions of biotite from metamorphic zones of northern England (Robinson et al. 1982; Spear 1995). **b** Retrograde zoning in biotite of an Ikulu metapelite (note low Ti values along the rims of biotite compared with the core). **c** P-T diagram showing calculated isopleths for total Al in amphibole in equilibrium with Zo, Di, Qz, and vapour (V) after Quirion and Jenkins (1998). Black box represents the P-T conditions for the formation of retrograde assemblage of calc-silicate rocks in Chemchem

of their morphology are interpreted to form pseudomorphs after kyanite (that is never preserved; Kazimoto et al. 2014a), or occurs intergrown with biotite. It is often surrounded by pinite pseudomorphs after cordierite (Fig. 4a, b). Minor minerals include zircon, monazite, ilmenite and magnetite. The zircon and monazite grains are surrounded by pleochroic haloes in the pinite, supporting the interpretation that the pinite is really formed after cordierite (Fig. 4b). The metapelite adjacent to the gold-bearing veins was affected by hydrothermal alteration of primary minerals, which includes chloritization of biotite, sericitization of plagioclase and sillimanite and the formation of epidote (Fig. 2).

Representative mineral analyses are presented in Table 1. The biotite in the metapelite exhibits X_{Fe} ratios of 0.44–058 (X_{Fe} = Fe/(Mg + Fe)). The titanium contents in biotite vary between 0.02 apfu along the rims to 0.15 apfu in the cores (Fig. 5a). Relict plagioclase is oligoclase containing an average X_{An} of 0.30. The hydrothermal sericite is muscovite, and the chlorite is ripidolite and pynochlorite (Table 1).

Calc-silicate rocks

Calc-silicate rocks crop out together with the metapelites. These rocks are rich in quartz (≈75 vol%) and diopside. Under the microscope, an assemblage of diopside, quartz and K-feldspar is partially replaced by a retrograde assemblage of tremolite, zoisite, muscovite and calcite. The

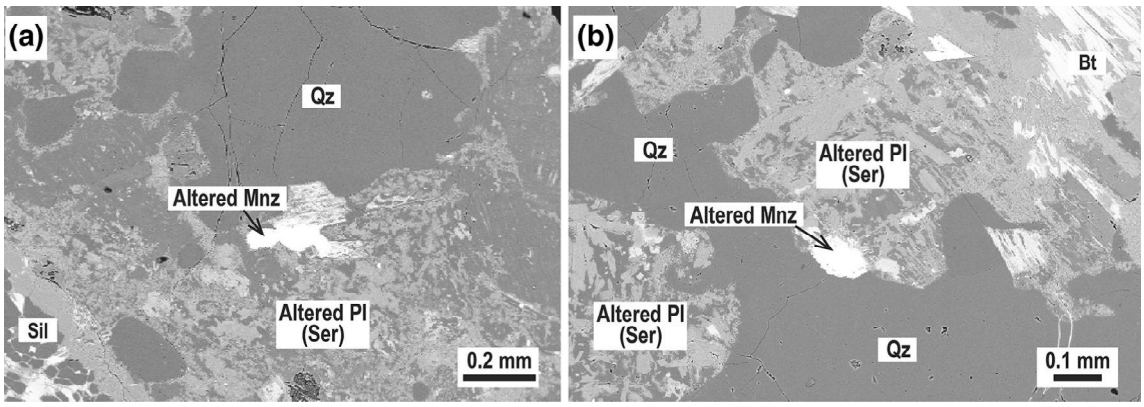


Fig. 6 Backscatter images of monazite grains (**a**, **b**) from the Ikulu metapelites showing the textural setting of hydrothermally altered monazite grains in the hydrothermally altered matrix of metapelites. BSE images of the monazite grains (**a**, **b**) can be seen in detail in Fig. 7c and d

zoisite is symplectitic intergrown with muscovite, albite and, in places, with calcite (Fig. 4c, d). Tremolite has an Al content of 0.51–0.04 apfu (Table 1) and is present as late-stage rims around diopside together with calcite. Additional minerals include titanite and zircon (Fig. 4c, d).

Orthoamphibolite

Orthoamphibolites are present near the Ikulu metapelites. This rock type contains hornblende, plagioclase and ilmenite. The hornblende is magnesiohornblende ($X_{Mg} = 0.56$) varying from olive green to brownish green and containing a mean TiO_2 content of about 1.0 wt% (0.1–0.13 Ti apfu.), 6.63 apfu Si and 0.47 apfu Al^{vi}. The plagioclase is labradorite ($X_{An} = 0.53$–0.57) and in part has been affected by later formation of sericite and epidote. Metabasites are discordantly cut by epidote–chlorite micro-veins, and the rocks next to the veins have been affected by hydrothermal alteration forming sericite, chlorite, epidote and calcite (Fig. 4e).

Metamorphic evolution of the vein country rocks at Chemchem

The mineralogy of the country rock of the Au–Cu–Pb veins reflects different stages of the metamorphic evolution prior to its hydrothermal alteration. These different evolutionary stages may also be recorded by the different internal growth zones and alteration textures of the monazite. The use of mineral chemistry data in determining the peak pressure and temperature conditions of metamorphism of the Ikulu metapelites at Chemchem is limited by the retrogression and hydrothermal alteration of its primary mineralogy, which led to the situation that cordierite is never preserved, but always completely pinitised. However, the common occurrence of cm-sized prismatic pseudomorphs of sillimanite after kyanite is evidence that the early stage of the evolution took place in the kyanite stability field. In contrast, the peak conditions are characterized by the formation of anatectic leucosomes and the stability of cordierite, sillimanite and K-feldspar. This suggests that the metapelites were subjected to high-grade metamorphic conditions of the upper amphibolite to granulite facies (e.g., Blümel and Schreyer 1977) during a later stage of its evolution. As the monazite grains included in garnet show a two-stage growth history, it can be concluded that the garnet prophyroblasts grew only during or after the second monazite growth stage, for which an age of 1,837 ± 6 Ma has been obtained (Kazimoto et al. 2014a), that is in agreement with the monazite age of 1,827 ± 10 Ma of this study. A detailed correlation between the growth history of the silicate minerals (kyanite stage versus garnet/cordierite-K-feldspar–sillimanite stage) and the two prograde growth zones of single monazite grains is presented in Kazimoto et al. (2014a).

The Ti-content and X_{Fe} values of biotite in metapelites are similar to those of biotite in kyanite–staurolite, sillimanite–staurolite and sillimanite–muscovite grades of metapelites in western Maine (USA; Fig. 5a; Robinson et al. 1982; Spear 1995). However, due to the strong retrograde exsolution of ilmenite, these mineral chemical data reflect only minimum metamorphic conditions. The influence of the retrogression on the Ti-content is seen in the strong decrease of the Ti-contents toward the rims of single biotite grains (Fig. 5b).

The hornblende–plagioclase thermometry of Holland and Blundy (1994) for the amphibolites requires that the Si content of the hornblende is <7.8 pfu and the plagioclase X_{An} is <92. Amphiboles and plagioclase in the clinopyroxene-bearing amphibolite of the present study meet those requirements. Estimates of the temperature using hornblende–plagioclase thermometry result in a temperature of amphibolite formation between 730 and 750 °C.

Retrograde formation of tremolite–zoisite–quartz from diopside and plagioclase in calc-silicate rocks and the maximum Al content of cores (0.51 pfu) of the late-stage tremolite are consistent with the formation of this retrograde assemblage at temperature and pressure conditions of about >650 °C and 7.6 kbar (Fig. 5c; Quirion and Jenkins 1998).

In summary, the textures and mineralogy of the hydrothermally altered metapelitic country rocks of the Au–Cu–Pb veins give evidence of two metamorphic stages during the prograde evolution, of which the first stage was in the kyanite stability field, whereas the peak metamorphism reached anatectic temperatures in the stability field of the

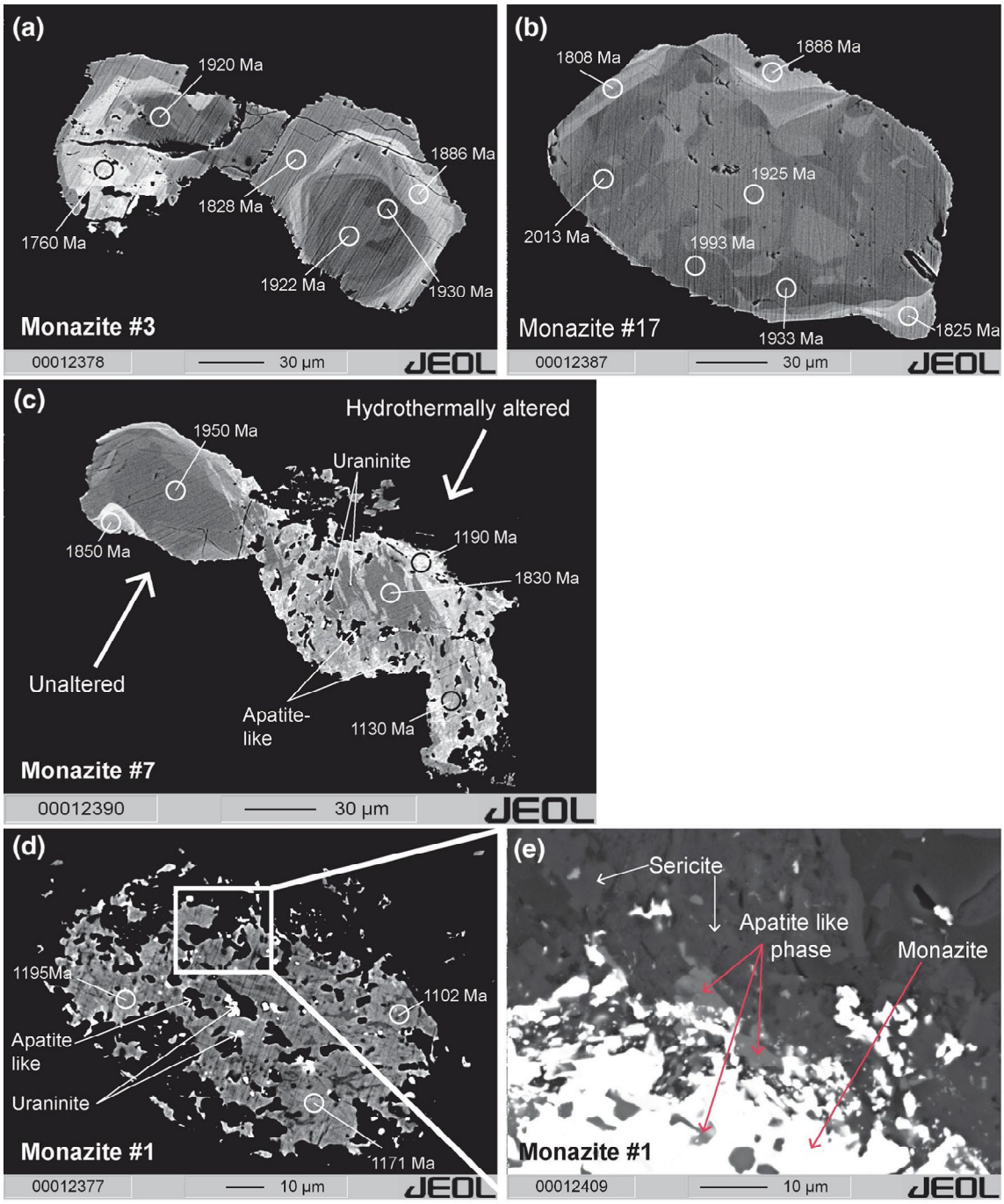


Fig. 7 Microtextures of selected monazite grains (in backscattered electron images; **a**–**e**): most metamorphic monazite grains display concentric (**a**) and patchy (**b**) zoning with overgrowths surrounding cores. The hydrothermal altered poikilitic monazite grains (**c**, **d**) are brighter than the metamorphic monazite (**c**) and contain inclusions of apatite-like phase and uraninite. **e** Large area of monazite displaying hydrothermally altered monazite, sericite and apatite-like phase

assemblage sillimanite–cordierite–biotite–K-feldspar. Estimates of peak temperatures of about 750 °C for this assemblage are in agreement with hornblende–plagioclase thermometry of a clinopyroxene-bearing amphibolite. Aluminum contents in late-stage tremolite of calc-silicates indicate partial retrograde re-equilibration below 660 °C at 7.6 kbar. The petrographic observations on different country rocks indicate that all rocks experienced similar high-grade metamorphic conditions and were only slightly affected by retrogression. No late-stage lower grade regional metamorphic overprint could be identified. The penetrative pinitization of cordierite and the sericitization of feldspars and sillimanite must have occurred under greenschist- to sub-greenschist-facies conditions and can be tentatively correlated with the hydrothermal alteration event. The same is true for chloritization of biotite and the epidote formation at expense of plagioclase. Texture and chemical changes of monazite due to the hydrothermal event are discussed in detail below.

Monazite in metapelite

Textures and chemistry

Unaltered and altered monazite is present in the matrix of the metapelites together with altered feldspars (sericite), pinite, sillimanite, biotite and quartz (Fig. 6a, b). In the altered metapelites, all minerals including monazite were affected to different degrees by hydrothermal alteration. Monazite occurs as inclusions in altered minerals and along grain boundaries. No textural relationship between the degree of alteration of monazite and its textural setting could be recognized with the possible exception that monazite inclusions in pinite tend to be better preserved. Monazite displays similar textures in all altered metapelites, of which two samples have been selected for detailed textural and mineral chemical analyses and dating of monazite. Backscatter electron images (BSE) of unaltered monazite grains show dark gray cores that display various zoning patterns (concentric and patchy; Fig. 7a, b) and are surrounded by bright, light gray to white overgrowths (Fig. 7a, b). The hydrothermally altered monazite is generally distinguishable from unaltered grains by its poikilitic texture and the bright and light gray color in BSE images (Fig. 7c–e). These altered grains include dark gray relicts of older monazite, bright white spots of uraninite and elongated black inclusions (Fig. 7c–e), which are rich in Ca and PO_4 and thus appear to be similar to apatite (Table 2; cf. Poitrasson et al. 2000).

The mineral chemistry data from the different types of monazite grains are presented in Tables 2 and in electronic supplementary tables 2–4. The altered and unaltered monazite grains exhibit different mineral chemical compositions. Compared with the chemistry of average unaltered overgrowth zones, the hydrothermally altered monazite has slightly higher Eu concentrations and is depleted in Y, U, Pb, Th, Er, Dy and Ca (Fig. 8). The Si levels in the altered monazite are variable, i.e., slightly higher or lower than that of the unaltered monazite, whereas the P and light rare earth elements (LREEs: La, Ce, Pr and Nd) are present at similar concentrations in both the altered and unaltered monazite (Fig. 8). In the plot of (Th + U+Si)*4 versus (REE + Y+P)*4 (Fig. 9), the unaltered monazite cores are characterized by cheralite substitution, whereas the unaltered monazite overgrowths plot between the huttonite and cheralite substitution vectors, suggesting effects of both substitutions on the unaltered overgrowths. In contrast, only the huttonite substitution vector is important in the hydrothermally altered monazite. The REE concentrations in the unaltered monazite cores and overgrown zones, exhibit similar chondrite normalized REE patterns (Fig. 10a, b). The heavy REE content in monazite of this garnet-free cordierite-bearing sample is not strongly depleted as one would expect if garnet grew together with monazite. The patterns of LREE are similar in all the three types of monazite grains. However, the altered monazite displays relatively depleted heavy rare earth element patterns (HREEs: Dy and Er) compared with those of the unaltered monazite cores and rims (Fig. 10a–c).

U–Th–total Pb monazite dating

Analyses of U, Th and total Pb concentrations in monazite were obtained from the hydrothermally altered metapelitic sample (T4-7-10). The results of 84 points of unaltered and 19 points of hydrothermally altered monazite were used to calculate the ages of the different monazite grains and growth zones. The resulting histograms are presented in Fig. 11. The three texturally and compositionally distinct monazite generations yielded three different weighted mean ages. The unaltered monazite cores have an age of 1,938 ± 11 Ma and the unaltered overgrowth zone an age of 1,827 ± 10 Ma. The hydrothermally altered monazite yielded a much younger age of 1,171 ± 17 Ma (Fig. 11).

Discussion

As the Ubendian Belt was affected by three orogenic events during the Paleoproterozoic, Mesoproterozoic and Neoproterozoic (Boniface et al. 2014, 2012; Boniface and Schenk 2012), we aimed to evaluate the possible role of these three events in the formation of the Mpanda Au–Cu–Pb mineralization. Our dating of the unaltered monazite cores and overgrowth zones in high-grade metapelites, which show concentric growth zones and patchy zoning due to dissolution–precipitation processes, yielded two

Table 2 Representative electron microprobe analyses of unaltered monazite cores, unaltered monazite overgrowth zones, hydrothermally altered monazite and an apatite-like phase

Analysis no.	Monazite									Apatite-like phase		
	Unaltered cores			Unaltered rim overgrowth			Hydrothermally altered					
	79	139	161	76	156	173	14	16	17	3	5	6
P_2O_5	29.08	30.57	28.82	27.49	30.15	29.63	29.39	29.96	30.00	34.61	30.50	38.16
SiO_2	0.84	0.11	1.31	1.67	0.34	0.83	0.84	0.33	0.32	0.48	0.17	0.32
CaO	0.80	1.40	1.00	0.72	0.61	0.67	0.19	0.32	0.32	31.64	36.59	44.58
La_2O_3	13.75	13.37	12.46	12.89	14.01	11.97	14.22	14.50	14.44	5.72	9.09	1.27
Ce_2O_3	28.68	27.20	25.28	28.73	29.35	27.13	29.33	30.35	30.67	11.96	12.46	4.22
Pr_2O_3	3.06	2.91	2.72	3.26	3.00	3.02	3.24	3.45	3.39	1.35	1.10	0.34
Nd_2O_3	11.95	11.19	10.82	12.24	11.62	12.40	13.05	13.30	13.40	5.30	4.91	1.52
Sm_2O_3	2.05	1.87	1.39	1.89	1.79	1.96	2.26	2.38	2.38	0.74	1.36	0.16
Eu_2O_3	bd	0.21	0.19	bd	0.06	bd	0.09	0.18	0.12	0.00	0.00	0.03
Gd_2O_3	1.57	1.60	1.28	1.19	1.54	1.91	1.71	1.75	1.67	0.55	0.67	0.38
Dy_2O_3	0.35	0.73	1.19	0.11	0.69	0.82	0.41	0.34	0.27	0.18	0.22	0.44
Y_2O_3	1.19	3.05	5.61	0.33	3.13	3.67	1.27	0.91	0.63	0.47	0.58	2.23
Er_2O_3	0.02	0.21	0.45	bd	0.23	0.25	0.04	0.02	bd	0.08	0.06	0.20
PbO	0.56	0.50	0.62	0.75	0.28	0.44	0.19	0.10	0.11	0.18	0.14	0.08
ThO_2	5.86	4.70	6.78	8.50	2.91	5.26	3.62	2.15	2.18	5.12	1.22	1.25
UO_2	0.32	0.30	0.11	0.27	0.15	0.05	0.03	0.02	0.01	0.09	0.00	0.11
Al_2O_3	0.01	0.00	0.00	0.01	0.00	0.00	0.00	0.00	0.00	0.01	0.02	0.00
Total	100.08	99.91	100.03	100.06	99.85	100.00	99.87	100.06	99.91	98.47	99.09	95.28
P	0.971	1.000	0.950	0.934	0.991	0.976	0.977	0.993	0.995	0.938	0.850	0.949
Si	0.033	0.004	0.051	0.067	0.013	0.032	0.033	0.013	0.012	0.015	0.006	0.009
Ca	0.034	0.058	0.042	0.031	0.025	0.028	0.008	0.013	0.013	1.085	1.291	1.403
La	0.200	0.191	0.179	0.191	0.201	0.172	0.206	0.209	0.209	0.068	0.110	0.014
Ce	0.414	0.385	0.360	0.422	0.417	0.386	0.422	0.435	0.440	0.140	0.150	0.045
Pr	0.044	0.041	0.039	0.048	0.042	0.043	0.046	0.049	0.048	0.016	0.013	0.004
Nd	0.168	0.155	0.150	0.176	0.161	0.172	0.183	0.186	0.188	0.061	0.058	0.016
Sm	0.028	0.025	0.019	0.026	0.024	0.026	0.031	0.032	0.032	0.008	0.015	0.002
Eu	bd	0.003	0.003	bd	0.001	bd	0.001	0.002	0.002	0.000	0.000	0.000
Gd	0.021	0.020	0.017	0.016	0.020	0.025	0.022	0.023	0.022	0.006	0.007	0.004
Dy	0.005	0.009	0.015	0.001	0.009	0.010	0.005	0.004	0.003	0.002	0.002	0.004
Y	0.025	0.063	0.116	0.007	0.065	0.076	0.027	0.019	0.013	0.008	0.010	0.035
Er	0.000	0.003	0.006	bd	0.003	0.003	0.001	0.000	bd	0.001	0.001	0.002
Pb	0.006	0.005	0.007	0.008	0.003	0.005	0.002	0.001	0.001	0.002	0.001	0.001

Table 2 continued

Analysis no.	Monazite									Apatite-like phase		
	Unaltered cores			Unaltered rim overgrowth			Hydrothermally altered					
	79	139	161	76	156	173	14	16	17	3	5	6
Th	0.053	0.041	0.060	0.078	0.026	0.047	0.032	0.019	0.019	0.037	0.009	0.008
U	0.003	0.003	0.001	0.002	0.001	0.001	0.000	0.000	0.000	0.001	0.000	0.001
Al	0.000	0.000	0.000	0.001	0.000	0.000	0.000	0.000	0.000	0.000	0.001	0.000
Total	2.003	2.005	2.012	2.008	2.002	2.001	1.997	1.999	1.998	2.386	2.525	2.496
X_{LREE}	0.081	0.798	0.740	0.052	0.848	0.805	0.900	0.916	0.924			
X_{HREE}	0.058	0.032	0.037	0.083	0.031	0.038	0.053	0.046	0.038			
X_{Hut}	0.442	−0.009	0.026	0.466	0.005	0.024	0.042	0.034	0.034			
X_{Brb}	0.414	0.116	0.083	0.391	0.051	0.056	0.000	0.000	0.000			
X_{YPO4}	0.006	0.063	0.115	0.008	0.065	0.076	0.005	0.004	0.003			
App. age (Ma)	1,925.5	1,931.0	1,941.7	1,897.7	1,858.2	1,825.0	1,156.3	1,076.1	1,153.8			
2σ err. age (±, Ma)	78.7	87.9	55.2	73.7	94.7	65.2	91.7	120.5	114.8			

bd below detection limit

metamorphic ages at about 1,940 and at 1,830 Ma. These two ages fall into the Paleoproterozoic orogenic cycle. The textures of the rock-forming minerals of the metapelites also indicate two stages during the prograde evolution: an early stage in the kyanite stability field and a younger stage in the sillimanite–cordierite–biotite–K-feldspar stability field. Although it was not possible to perform texturally controlled dating of the two metamorphic stages (due to the absence of true kyanite relicts), we tentatively correlate the two Paleoproterozoic monazite ages with the kyanite stage (1,940 Ma) and the sillimanite-cordierite stage (1,830 Ma), respectively (for more details, see Kazimoto et al. 2014a).

The older metamorphic age (ca. 1,940 Ma) is similar to reported metamorphic zircon and monazite ages in different blocks of the Ubendian Belt (Boniface et al. 2012; Lawley et al. 2013b, c; Kazimoto et al. 2014b). It is interpreted to correlate with pre-collisional accretionary processes (Kazimoto et al. 2014a). Also the younger metamorphic monazite age (ca. 1,830 Ma) found in the Chemchem metapelite, has already been recognized in the Ufipa and Ubende Blocks (Boniface and Schenk 2012; Boniface et al. 2012). It postdates the formation of MORB-type eclogites (ca. 1,880 Ma) of the Ubende Block (Boniface et al. 2012) and is correlated with the collision event (Kazimoto et al. 2014a). Unlike the prograde metamorphic monazite, the hydrothermally altered monazite is only found in metapelite samples bordering the gold-bearing veins (Fig. 7c–e).

Our interpretation that the poikilitic, inclusion-rich monazite grains have been formed by hydrothermal fluids is similar with interpretation of textures described by Hetherington and Harlov (2008), who demonstrated formation of phases like uraninite, thorite and apatite from monazite. A fluid-assisted dissolution–precipitation mechanism is thought to be responsible to produce such replacements textures. Experimental results of Ayers and Watson (1991) and Ayers et al. (2004) indicate that P, T and pH have a strong influence on the solubility of monazite in hydrothermal fluids. In addition, the nature of ligands (F^-, OH^-, Cl^- and CO^{3+}) is certainly a further important parameter. The lowest solubility is at neutral pH values but is increasing toward acidic and toward alkaline conditions as well. This indicates that monazite may dissolve in acidic hydrothermal fluids that cause sericitization of rocks (Poitrasson et al. 2000). Since sericitization of, e.g., feldspars leads to increasing pH values of the hydrothermal fluid (Gruner 1944), new monazite may precipitate together with sericite from the neutral or less acidic fluid. Besides this dissolution–precipitation mechanism also cation exchange between the existing monazite and the hydrothermal fluids may lead to the formation of a new isotopically reset hydrothermal monazite (Harlov et al. 2005). The cation exchange

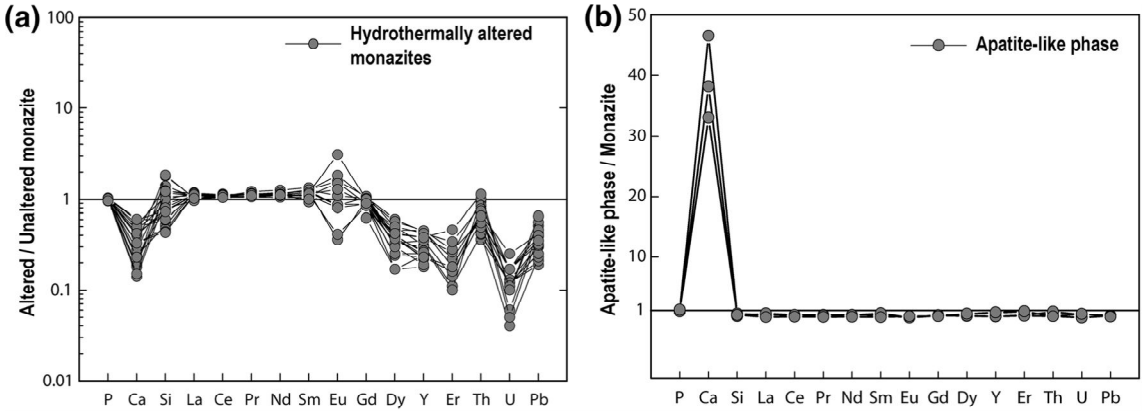


Fig. 8 Comparison of concentrations of various elements in hydrothermally altered monazite and an apatite-like phase with unaltered monazite overgrowths. **a** HREEs, U, Pb, Ca and Th are depleted in hydrothermally altered monazite compared with unaltered overgrowths; Eu is variable in hydrothermally altered monazite and P and LREE concentrations are similar in hydrothermally altered and unaltered monazite. **b** The apatite-like phase has similar concentrations of elements as unaltered monazite except for Ca

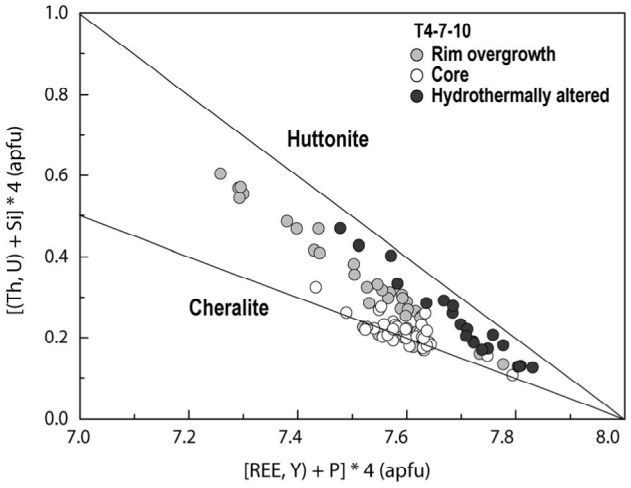


Fig. 9 Plot of ((Th, U) + Si)*4 versus ((REEs, Y) + P)*4 showing cheralite and huttonite vectors

may follow the known cheralite ($2REE^{3+} = Th^{4+} + Ca^{2+}$) and huttonite ($REE^{3+} + P^{5+} = Th^{4+} + Si^{4+}$) substitutions (Pyle et al. 2001).

In addition to these hydrothermal recrystallization mechanisms of monazite, Poitrasson et al. (2000) described also different replacements of monazite grains by other minerals as an apatite-like phase, allanite or pyrite. From these different mechanisms, the apatite-like replacement occurred also in the Chemchem-altered metapelite as evidenced by the numerous apatite-like inclusion associated with uraninite in the hydrothermally altered sieve-like monazite grains (Fig. 7c–e). Interestingly, the host monazite showing the apatite-like replacement is characterized by Ca, Gd, Dy and Y-depletion (Fig. 8a). This indicates that the altered monazite may have acted as a source for these elements during the formation of the apatite-like phase (cf. Didier et al. 2013; Harlov et al. 2005), which has the similar concentration of the elements as unaltered monazite (Fig. 8a, b). The replacement of pristine monazite by newly formed monazite with another composition and by new phases such as apatite and uraninite is the best textural argument to attest that poikilitic monazite have been formed by fluid-assisted dissolution-precipitation (Harlov et al. 2010). The uraninite crystallization implies that uranium was mobilized by oxidant fluid.

The presence of inherited and/or common Pb in altered monazite is possible; however, the low Pb content of the newly formed monazite (Fig. 12) suggests that the obtained age reflects indeed the true age of its crystallization. In addition, the age of the hydrothermally altered monazite is in agreement with the age of metamorphism of the adjoining Wakole Block (ca. 1,170 Ma) and supports the interpretation that the fluid–rock interaction, which is associated with both the hydrothermal alteration of the metapelite and the deposition of Au, Cu and Pb in the veins, actually occurred in the Mesoproterozoic and thus correlates with the age of the Kibaran orogenic belt adjoining the Ubendian Belt to the west. This orogeny has also affected the Paleoproterozoic rocks of some parts of the Ubendian Belt (Boniface et al. 2012, 2014). However, our petrographic and dating study of country rocks of the gold-bearing veins at Chemchem in the Katuma Block, which include metapelites, calc-silicate rocks and metabasites, revealed that these rocks experienced only high-grade metamorphic events of Paleoproterozoic ages but no lower grade overprints during the Mesoproterozoic orogeny. In addition, the mineral assemblages of the

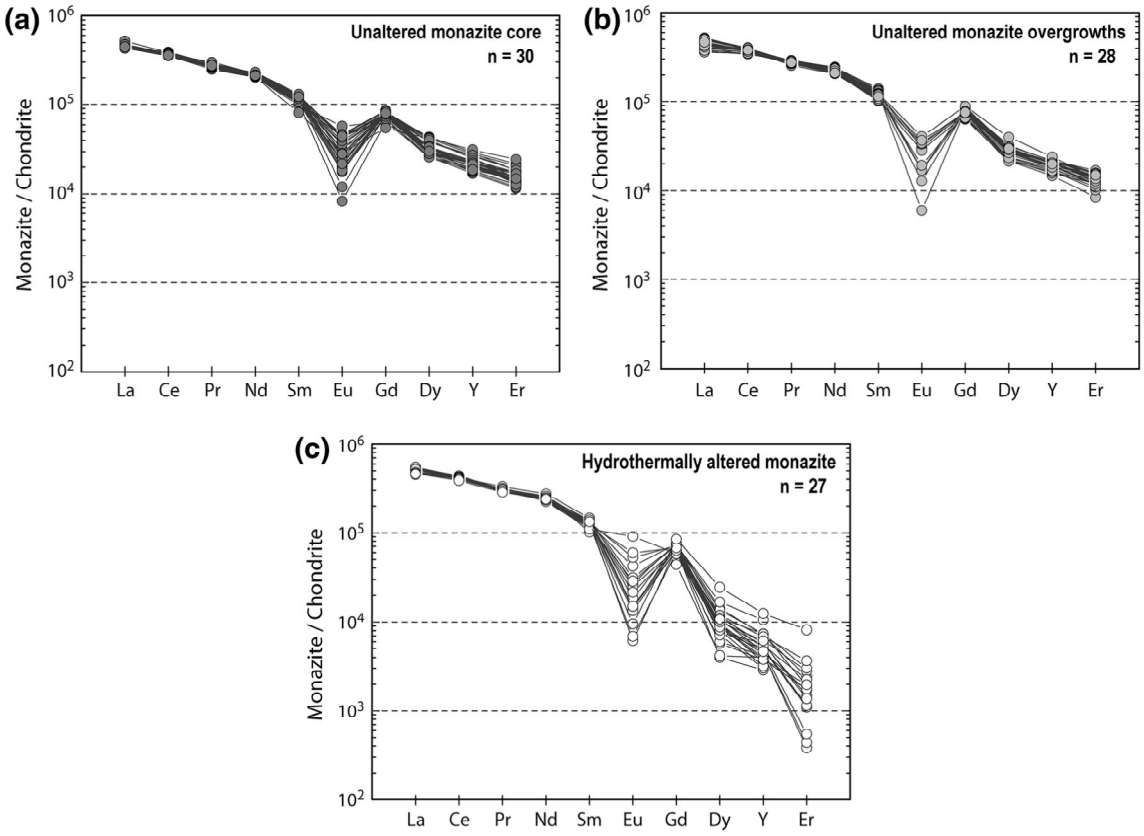


Fig. 10 Chondrite-normalized REE and Y patterns of the three types of monazite in the Chemchem metapelite; the normalizing values are from McDonough and Sun (1995)

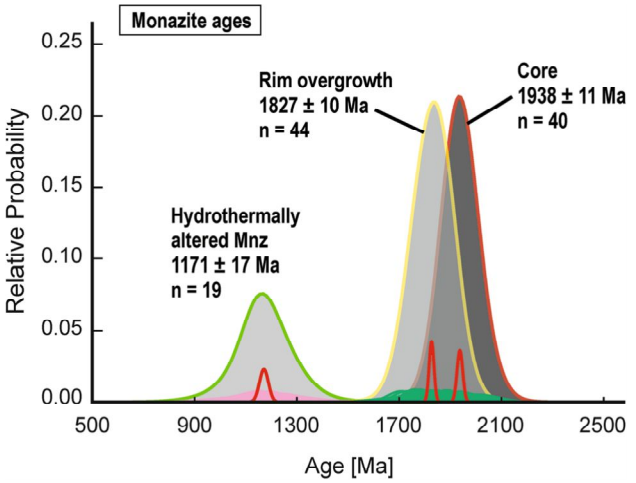


Fig. 11 Age histograms: the tall curves (*red*, *yellow* and *green*) are sum curves for the date of each age population, and the short curves (*red*) are curves for the weighted mean age (2σ error) of the age populations

different vein host rocks (e.g., metapelites, calc-silicate rocks, metabasites) are not rich in volatiles and can be excluded as source rocks for the fluids (H_2O and CO_2) from which the hydrothermal carbonate–quartz veins were formed.

Importantly, dating of monazite and zircon from metapelites of the tectonically adjoining Wakole Block of the Ubendian Belt (Fig. 1; Smirnov et al. 1970) yielded a remarkably similar age of 1,170 ± 10 Ma of their first amphibolite grade metamorphism during crustal thickening (Boniface et al. 2014). The agreement between the age of the hydrothermal alteration in the Katuma Block with that of the first metamorphism of the Wakole sediments suggests that the release of fluids from the fluid–fertile sediments during this crustal-thickening event most likely generated the hydrothermal fluids required for the formation of the Au–Cu–Pb deposits in the tectonically adjoining Katuma Block. Similar ages (ca. 1,180–1,090 Ma) have also been reported for the metamorphic overprinting of the rocks of the Ubende Block (Boniface et al. 2012). The age of the compressional event found in the Wakole and Ubende Blocks is in agreement with the model of Fernandez-Alonso et al. (2012), according to which the closing of intra-cratonic basins and the formation of the Kibaran orogenic belt in east and central Africa during Mesoproterozoic time (ca. 1.0 Ga) was driven by far-field

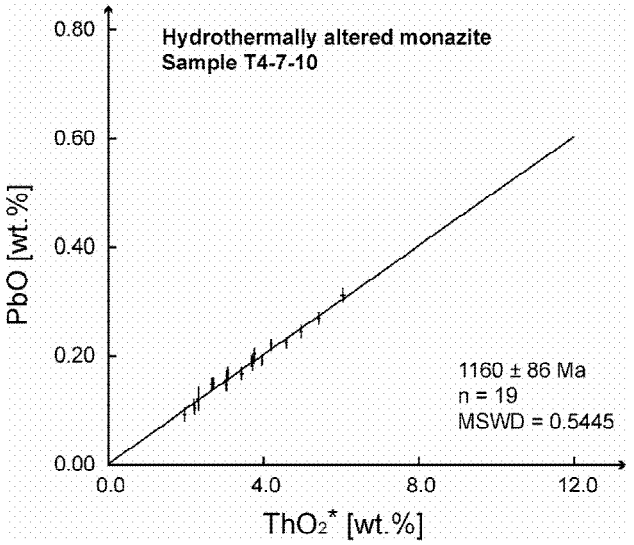


Fig. 12 ThO_2* versus PbO diagram showing an isochron plotted for hydrothermally altered monazite. The Pb content (inherited and/or common) during crystallization was very low. The monazite age obtained from the isochron diagram (after Suzuki and Adachi 1991) is slightly younger and has a larger error than the ages shown in the *histogram* (after Montel et al. 1996)

compressional forces related to the amalgamation of the Rodinia supercontinent.

Summary and conclusions

In situ U–Th–total Pb dating of monazite grains of hydrothermally altered high-grade metapelites, forming the country rocks of Au–Cu–Pb veins in the Katuma Block of the Ubendian Belt yielded two metamorphic ages of about 1,940 Ma and 1,830 Ma. As these metamorphic ages are well established for several blocks of the Ubendian Belt, it indicates that the monazite of the hydrothermally altered metapelites preserved the original mineral crystallization ages obtained during prograde Paleoproterozoic metamorphic events. In addition to these unaltered Paleoproterozoic monazite grains, the metapelites contain hydrothermally altered monazites grains that are chemically and texturally distinct and contain relicts of the older metamorphic grains or growth zones. This new hydrothermally crystallized monazite gives Mesoproterozoic ages of about 1,170 Ma that correlate with metamorphic ages obtained for the first amphibolite facies metamorphism of metapelites of the Wakole Block. This block is in tectonic contact with the Katuma Block hosting the hydrothermal Au–Cu–Pb deposits. The hydrothermal event coincides with the Mesoproterozoic crustal thickening and shortening that led to the formation of the Kibaran orogenic belt bordering the Ubendian Belt to the west. Our new radiometric age indicates that under-thrusting of metasediments of the adjoining Wakole Block below the rocks of the Katuma Block most likely triggered metamorphism and dehydration of the sediments of the Wakole Block and generated fluids that percolated through the rocks of the Katuma Block and concentrated metals in the veins. The age of the hydrothermal event proposed here is younger than the earlier proposed Pb–Pb sulfides model age of ca. 1,660 Ma and older than the Pb–Pb model age of ca. 720 Ma for the mineralization event in the Katuma Block. Moreover, this age is younger than that of the gold mineralization event in the Lupa Block at the southern part of the Ubendian Belt, which was dated at ca. 1,950–1,940 and at 1,880 Ma with the Re–Os method using sulfides (Lawley et al. 2013c). The distinct mineralization ages in the Katuma and Lupa Block indicate that the poly-orogenic Ubendian Belt was at least twice affected by mineralization events.

Acknowledgments The authors would like to thank the Ministry of Education and Vocational Training of Tanzania (MOEVT), the German Academic Exchange Service (DAAD) and the Department of Geology of the University of Dar es Salaam, Tanzania (through the Sida Earth Science Project), for providing funding for this research. We are grateful to Andreas Fehler and Barbara Mader for their service at the laboratories of the Christian-Albrechts-Universität Kiel.

References

Appel P (2010) "AgeFinder": a Mac OS X computer program to evaluate electron microprobe data of monazite for chemical age dating. Comput Geosci 36:559–563

Appel P (2013) CombError. http://www.ifg.uni-kiel.de/339.html. Accessed 18 Jan 2014

Armstrong JT (1995) CITZAF: a package of correction programs for the quantitative electron microbeam X-ray analysis of thick polished materials, thin films, and particles. Microbeam Anal-Deerfield Beach 4:177–200

Arne DC, Morgan JW, Stein HJ, Bierlein FP (2001) Re–Os dating of sulfides associated with gold mineralization in central Victoria, Australia. Econ Geol 96:1455–1459

Ayers JC, Watson EB (1991) Solubility of apatite, monazite, zircon, and rutile in supercritical aqueous fluids with implications for subduction zone geochemistry. Philos Trans R Soc A: Math Phys Eng Sci 335:365–375

Ayers JC, Loflin M, Miller CF, Barton MD, Coath C (2004) Dating fluid infiltration using monazite. Proc Eleventh Int Symp Water–Rock Interact 1:247–251

Barley ME, Groves DI (1992) Supercontinent cycles and the distribution of metal deposits through time. Geology 20:291–294

Biyashev M, Pentelkov V, Emelyanov S, Chuklanov B, Stepnov E, Matrenitzky T, Novikov A (1977) Sitalike: geological map quarter degree sheet 170. Geological Survey of Tanzania, Dodoma

Blümel P, Schreyer W (1977) Phase Relations in Pelitic and Psammitic Gneisses of the Sillimanite—Potash Feldspar and Cordierite-Potash Feldspar Zones in the Moldanubicum of the Lam—Bodenmais Area, Bavaria. J Petrol 18:431–459

Boniface N, Schenk V (2012) Neoproterozoic eclogites in the Paleoproterozoic Ubendian Belt of Tanzania: evidence for a Pan-African suture between the Bangweulu Block and the Tanzania Craton. Precambrian Res 208–211:72–89

Boniface N, Schenk V, Appel P (2012) Paleoproterozoic eclogites of MORB-type chemistry and three Proterozoic orogenic cycles in the Ubendian Belt (Tanzania): evidence from monazite and zircon geochronology, and geochemistry. Precambrian Res 192–195:16–33

Boniface N, Schenk V, Appel P (2014) Mesoproterozoic high-grade metamorphism in pelitic rocks of the northwestern Ubendian Belt: implication for the extension of the Kibaran intra-continental basins to Tanzania. Precambrian Res 249:215-228

Boven A, Theunissen K, Sklyarov E, Klerkx J, Melnikov A, Mruma AH, Punzalan L (1999) Timing of exhumation of a high-pressure mafic granulite terrane of the Paleoproterozoic Ubende belt (West Tanzania). Precambrian Res 93:119–137

Braun I, Appel P (2006) U–Th–total Pb dating of monazite from orthogneisses and their ultra-high temperature metapelitic enclaves: implications for the multistage tectonic evolution of the Madurai Block, southern India. Eur J Miner 18:415–427

Cahen L, Snelling NJ, Delhal J, Vail J (1966) The geochronology and evolution of Africa. Clarendon Press, Oxford

Daly MC (1988) Crustal shear zones in Central Africa: a kinematic approach to Proterozoic Tectonics. Episodes 11:5–11

Davis DW, Schandl ES, Wasteneys HA (1994) U–Pb dating of minerals in alteration halos of Superior Province massive sulfide deposits: syngenesis versus metamorphism. Contrib Miner Petrol 115:427–437

Delvaux D (2001) Tectonic and palaeostress evolution of the Tanganyika-Rukwa-Malawi rift segment, East African rift System. Peri-Tethys Memoir 6: Peri—Tethyan Rift/Wrench Basins and Passive Margins, vol 6. Mimoires du Museum national d'Histoire naturelle, Paris

Didier A, Bosse V, Boulvais P, Bouloton J, Paquette JL, Montel JM, Devidal JL (2013) Disturbance versus preservation of U–Th–Pb ages in monazite during fluid–rock interaction: textural, chemical and isotopic in situ study in microgranites (Velay Dome, France). Contrib Miner Petrol 165:1051–1072

Donovan JJ, Hanchar JM, Picolli PM, Schrier MD, Boatner LA, Jarosewich E (2003) A re-examination of the rare-earth-element orthophosphate standards in use for electron-microprobe analysis. Can Mineral 41:221–232

Fernandez-Alonso M, Cutten H, De-Waele B, Tack L, Tahon A, Baudet D, Barritt SD (2012) The Mesoproterozoic Karagwe–Ankole Belt (formerly the NE Kibara Belt): the result of prolonged extensional intracratonic basin development punctuated by two short-lived far-field compressional events. Precambrian Res 216–219:63–86

Frei R, Pettke T (1996) Mono-sample Pb–Pb dating of pyrrhotite and tourmaline: proterozoic vs. Archean intracratonic gold mineralization in Zimbabwe. Geology 24:823–826

Goldfarb RJ, Groves DI, Gardoll S (2001) Orogenic gold and geologic time: a global synthesis. Ore Geol Rev 18:1–75

Gruner JW (1944) The hydrothermal alteration of feldspars in acid solutions between 300 degrees and 400 degrees C. Econ Geol 39:578–589

Harlov DE, Wirth R, Förster H-J (2005) An experimental study of dissolution–reprecipitation in fluorapatite: fluid infiltration and the formation of monazite. Contrib Miner Petrol 150:268–286

Harlov DE, Wirth R, Hetherington CJ (2010) Fluid-mediated partial alteration in monazite: the role of coupled dissolution–reprecipitation in element redistribution and mass transfer. Contrib Miner Petrol 162:329–348

Hetherington CJ, Harlov DE (2008) Metasomatic thorite and uraninite inclusions in xenotime and monazite from granitic pegmatites, Hidra anorthosite massif, southwestern Norway: mechanics and fluid chemistry. Am Mineral 93:806–820

Holland TJB, Blundy JD (1994) Non-ideal interactions in calcic amphiboles and their bearing on amphibole–plagioclase thermometry. Contrib Miner Petrol 116:433–447

Horstwood MSA, Foster GL, Parrish RR, Noble SR, Nowell GM (2003) Common-Pb corrected in situ U–Pb accessory mineral geochronology by LA-MC-ICP-MS. J Anal At Spectrom 18:837–846

Hu F, Fan H, Yang J, Wan Y, Liu D, Mingguo Z, Chengwei J (2004) Mineralizing age of the Rushan lode gold deposit in the Jiaodong Peninsula: SHRIMP U–Pb dating on hydrothermal zircon. Chin Sci Bull 49:1629–1636

Jarosewich E, Boatner LA (1991) Rare-earth-elements reference samples for electron microprobe analysis. Geostand Newsl 15:397–399

Jöns N, Schenk V, Appel P, Razakamanana T (2006) Two-stage metamorphic evolution of the Bemarivo Belt of northern Madagascar: constraints from reaction textures and in situ monazite dating. J Metamorph Geol 24:329–347

Kazimoto EO, Schenk V, Appel P (2014a) Granulite-facies metamorphic events in the northeastern Ubendian Belt of Tanzania: implications for the Neoarchean to Paleoproterozoic crustal evolution. Precambrian Res 256:31–47

Kazimoto EO, Schenk V, Berndt J (2014b) Neoarchean and Paleoproterozoic crust formation in the Ubendian Belt of Tanzania: insights from zircon geochronology and geochemistry. Precambrian Res 252:119–144

Kerrich R, Cassidy KF (1994) Temporal relationships of lode gold mineralization to accretion, magmatism, metamorphism and deformation—Archean to present: a review. Ore Geol Rev 9:263–310

Kerrich R, Kyser TK, Kyser KT, Kurt KT (1994) 100 Ma timing paradox of Archean gold, Abitibi greenstone belt (Canada): new evidence from U–Pb and Pb–Pb evaporation ages of hydrothermal zircons. Geology 22:1131–1134

Kilembe EA, Rosendahl BR (1992) Structure and stratigraphy of the Rukwa rift. Tectonophysics 209:143–158

Lawley CJM, Imber J, Selby D (2013a) Structural controls on orogenic Au mineralization during transpression: Lupa Goldfield, Southwestern Tanzania. Econ Geol 108:1615–1640

Lawley CJM, Selby D, Condon DJ, Horstwood M, Millar I, Crowley Q, Imber J (2013b) Lithogeochemistry, geochronology and geodynamic setting of the Lupa Terrane, Tanzania: implications for the extent of the Archean Tanzanian Craton. Precambrian Res 231:174–193

Lawley CJM, Selby D, Condon DJ, Imber J (2013c) Palaeoproterozoic orogenic gold style mineralization at the Southwestern Archaean Tanzanian cratonic margin, Lupa Goldfield, SW Tanzania: implications from U–Pb titanite geochronology. Gondwana Res 26(3–4):1141–1158

Lawley CJM, Selby D, Imber J (2013d) Re–Os molybdenite, pyrite and chalcopyrite geochronology, Lupa Goldfield, Southwestern Tanzania: tracing metallogenic time scales at midcrustal shear zones hosting orogenic Au deposits. Econ Geol 108:1591–1613

Lenoir JL, Liégeois JP, Theunissen K, Klerkx J (1994) The Palaeoproterozoic Ubendian shear belt in Tanzania: geochronology and structure. J Afr Earth 19:169–184

McDonough WF, Sun SS (1995) The composition of the Earth. Chem Geol 120:223–253

Montel JM, Foret S, Veschambre M, Nicollet C, Provost A (1996) Electron microprobe dating of monazite. Chem Geol 131:37–53

Nanyaro JT (1989) Proterozoic gold-base metal veins in the Mpanda mineral field, western Tanzania. Annales Series in-8, Science Geologiques, vol 97. Musée Royale de L'Afrique Centrale, Tervuren, Belgium, p 144

Oelkers EH, Poitrasson F (2002) An experimental study of the dissolution stoichiometry and rates of a natural monazite as a function of temperature from 50 to 230 °C and pH from 1.5 to 10. Chem Geol 191:73–87

Paquette JL, Tiepolo M (2007) High resolution (5 μm) U–Th–Pb isotope dating of monazite with excimer laser ablation (ELA)-ICPMS. Chem Geol 240:222–237

Phillips D, Miller JM (2006) 40Ar/39Ar dating of mica-bearing pyrite from thermally overprinted Archean gold deposits. Geology 34:397

Poitrasson F, Chenery SC, Shepherd TJ (2000) Electron microprobe and LA-ICP-MS study of monazite hydrothermal alteration: implications for U–Th–Pb geochronology and nuclear ceramics. Geochim Cosmochim Acta 64:3283–3297

Pohl W (1994) Metallogeny of the northeastern Kibara belt, Central Africa-Recent perspectives. Ore Geology Rev 9:105-130

Pyle JM, Spear FS, Rudnick RL, Mcdonough WF (2001) Monazite–xenotime–garnet equilibrium in metapelites and a new monazite–garnet thermometer. J Petrol 42:2083–2107

Quirion DM, Jenkins DM (1998) Dehydration and partial melting of tremolitic amphibole coexisting with zoisite, quartz, anorthite, diopside, and water in the system H_2O–CaO–MgO–Al_2O_3–SiO_2. Contrib Miner Petrol 130:379–389

Rasmussen B, Sheppard S, Fletcher IR (2006) Testing ore deposit models using in situ U–Pb geochronology of hydrothermal monazite: Paleoproterozoic gold mineralization in northern Australia. Geology 34:77

Ring U, Kröner A, Toulkeridis T (1997) Palaeoproterozoic granulite-facies metamorphism and granitoid intrusions in the Ubendian–Usagaran Orogen of northern Malawi, east-central Africa. Precambrian Res 85:27–51

Robinson P, Hollocher K, Tracy R, Dietsch C (1982) High grade Acadian regional metamorphism in south-central Massachusetts. In: Joester RA, Quarrier SS (eds) NEIGC 74th Annual Meeting of the state Geological and Natural History Survey of Connecticut, guidebook for fieldtrips in Connecticut and South-Central Massachusetts, 1982, pp 289–340

Selby D, Creaser RA, Hart CJRR, Rombach CS, Thompson JFHH, Smith MT, Bakke AA, Goldfarb RJ (2002) Absolute timing of sulfide and gold mineralization: a comparison of Re–Os molybdenite and Ar–Ar mica methods from the Tintina Gold Belt, Alaska. Geology 30:791–794

Semyanov A, Kireev A, Doronkin I, Gavrilov G, Matrenitzky T, Novicov AG (1977) Mpanda: geological map quarter degree sheet 153. Geological Survey of Tanzania, Dodoma

Smirnov V, Shulyatin O, Tolochko V, Zhukov S, Mwakisunga M, Matrenitzky T (1970) Katuma: geological map quarter degree sheet 152. Ministry of Energy and Minerals, Dodoma

Spear FS (1995) Metamorphic phase equilibria and pressure–temperature–time paths. Mineralogical Society of America, Washington

Stein HJ, Markey RJ, Morgan JW, Hannah JL, Schersten A (2001) The remarkable Re–Os chronometer in molybdenite: how and why it works. Terra Nova 13(6):479–486

Stendal H, Frei R, Muhongo S, Rasmussen TM, Mnali SR, Petro F, Brian Temu E (2004) Gold potential of the Mpanda mineral field, SW Tanzania: evaluation based on geological, lead isotopic and aeromagnetic data. J Afr Earth Sci 38:437–447

Suzuki K, Adachi M (1991) Precambrian provenance and Silurian metamorphism of the Tsubonosawa paragneiss in the South Kitakami terrane, Northeast Japan, revealed by the chemical Th–U–total Pb isochron ages of monazite, zircon and xenotime. Geochem J 25(5):357–376

Theunissen K, Klerkx J, Melnikov A, Mruma AH (1996) Mechanisms of inheritance of rift faulting in the western branch of the East African Rift, Tanzania. Tectonics 15:776–790

Vielreicher NM, Groves DI, Fletcher IR, McNaughton NJ, Rasmussen B (2003) Hydrothermal monazite and xenotime geochronology: a new direction for precise dating of orogenic gold mineralization. Soc Econ Geol 53(1):10–16